# GROUND TRUTH IN CENTRAL ASIA FROM IN-COUNTRY NETWORKS

Gaspar Monsalve[1], Anne F. Sheehan[1], Thomas de la Torre[1], Charlotte Rowe[2], and Michael Begnaud[2]

University of Colorado at Boulder[1] and Los Alamos National Laboratory[2]

Sponsored by National Nuclear Security Administration
Office of Nonproliferation Research and Engineering
Office of Defense Nuclear Nonproliferation

Contract Nos. DE-FC52-04NA25544[1] and W-7405-ENG-36[2]

## ABSTRACT

We improve regional velocity structure and the database of seismic event ground truth (GT) information for central and southern Asia using data from a recent broadband seismic experiment in the Himalayas and the southern Tibetan Plateau, supplemented by local network data and other regional data. GT events can be used to calibrate station-centric correction surfaces and increase the ability to accurately locate and identify seismic events in these regions. In central Asia, limited station coverage results in poor reference-event coverage. The Himalayan Nepal Tibet Seismic Experiment (HIMNT) consisted of 29 broadband STS2 seismometers deployed in eastern Nepal and southern China (2001–2003). The data set is unique, with many stations in remote and difficult to access locations. GT coverage is sparse, and no permanent stations exist in most of the area covered by our network.

We have examined the entire continuous HIMNT seismic data set and have located >1600 regional and local events with magnitudes between 1 and 5.5. Initial hypocenters were determined using *a priori* one-dimensional (1D) velocity models and a weighted least squares location algorithm. We further refined the earthquake hypocenters using double-difference schemes and iterative three-dimensional (3D) velocity tomography with earthquake relocation. We have applied joint inversion routines to the >1600 earthquakes to solve simultaneously for hypocenters and seismic velocity structure. The code VELEST was used to determine best fitting 1D velocity models for the Himalayas and the southern Tibetan Plateau. We have found high velocities in the Tibetan lower crust and low Vp/Vs in the upper crust beneath the Tibetan Plateau. We also found a >15-km difference in crustal thickness between the Lesser Himalaya and the Tibetan Plateau. Receiver function analysis further constrains the crustal thickness variations. This large velocity heterogeneity over a small lateral distance makes a 3D velocity model important for determining accurate hypocenters. The code SIMUL2000 was then used to determine 3D velocity structure and iteratively relocate events in the new 3D velocity model. Earthquake hypocenters delineate several distinct groupings that correlate with collision zone tectonics. Crustal earthquakes show alignments with depths <25 km along the Himalayan Front's region of highest relief. Clusters of upper mantle earthquakes are found beneath the High Himalaya, in the Tethyan Himalaya, and beneath southern Nepal. We observe earthquake hypocenters over a range of depths, beneath Nepal from near-surface to 65 km deep and beneath the Tibetan Plateau from near-surface to 90 km deep. Although events cluster with depth, there are no large depth-distribution gaps.

Developing our GT catalog includes supplementing HIMNT data with other network data, along with moment tensor and source parameter analysis of GT events, with particular attention to depth control. We determined focal mechanisms using waveforms and first motions from 17 of the largest, best-recorded local earthquakes during the HIMNT experiment. We used a regional waveform moment tensor inversion method and first-motion polarities obtained from HIMNT, Nepal Department of Mines and Geology (DMG), and the Program for Array Studies of the Continental Lithosphere (PASSCAL) network deployed in Bhutan (2001–2003). Waveform solutions were obtained using HIMNT, Bhutan PASSCAL, and GSN (Lhasa) data. We performed a grid search over source depth to examine the sensitivity of the moment tensor solution to event depth and to find the best fitting source depth. We performed inversions using a range of passbands. Crosschecking focal mechanisms from full waveform moment with first-motion solutions revealed good agreement. We found that normal faulting with extensional axes trending E-W is common in the Tibetan Plateau's upper crust and that many earthquakes occur beneath the Moho, most having strike-slip mechanisms with compressional axes trending NW-SE to NE-SW. The new GT events can be used to calibrate station-centric correction surfaces and increase the ability to accurately locate and identify seismic events in these regions.

## OBJECTIVES

The goals of this project are (1) to contribute to the database of GT seismic events in central Asia using data from the HIMNT network and other regional seismic data and (2) to determine detailed seismic body-wave velocity models for the portion of central Asia covered by the HIMNT network.

## RESEARCH ACCOMPLISHED

### HIMNT deployment

The HIMNT was a National Science Foundation PASSCAL deployment in Nepal and Tibet during 2001–2003 (Figure 1). HIMNT was the first broadband seismic experiment to cover the plains of southern Nepal, the Lesser and Greater Himalaya, and the Southern Tibetan Plateau simultaneously. The HIMNT experiment included the deployment of 29 three-component broadband seismic stations, which recorded continuously at a sample rate of 40 sps. Although the project primarily has tectonic objectives, the high-quality data collected is ideal for GT data for monitoring purposes. HIMNT stations were installed with approximately 40–50 km station spacing, covering a two-dimensional area approximately 300 km wide east-west by 300 km north-south (Figure 1). This geometry is well suited for both event location and seismic velocity structure projects. Station locations were dictated strongly by logistics, with some stations only accessible by air or by a several-day hike on foot.

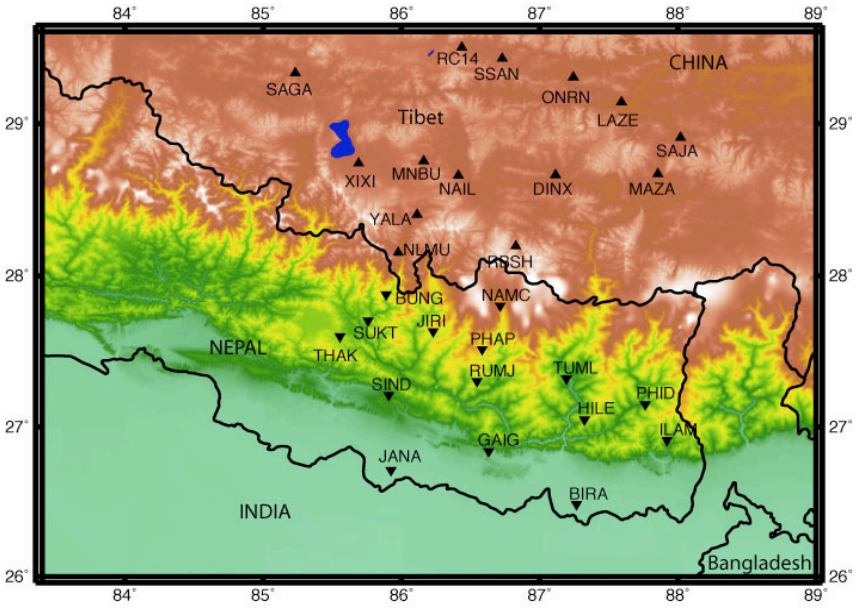


**Figure 1. Topographic map with broadband seismic stations of the 2001–2003 Himalayan Nepal Tibet PASSCAL Seismic Experiment.**

### Initial locations

After identifying times for all the first P- and S-wave arrivals from the HIMNT continuous data set of seismograms, hypocenters were determined for 1651 local earthquakes. Earthquake hypocenters were first determined using the ANTELOPE software of Boulder Real Time Technologies. In particular, we used the ANTELOPE routine dbgenloc, which utilizes a weighted least-squares method using a three-layer *a priori* velocity model in order to determine earthquake hypocenters given first arrival travel times. All travel time arrivals were used in the hypocentral inversion, and each event was located individually. Weight was assigned to every arrival according to the length of the error window given to the pick and the event-station distance. Local magnitudes were calculated for all the earthquakes and ranged from 1 to 5.5. Moment magnitudes were also calculated for a subset of earthquakes with high-quality seismograms for which full waveform moment tensor inversions were performed. Comparison of these two kinds of independently estimated magnitudes shows a good agreement between the two, though the local magnitudes are on average larger by one-fifth of a magnitude unit compared to the moment magnitudes (Figure 2).

Figure 3 shows a magnitude-frequency diagram for our network, which can be used to estimate our detection threshold and catalog completeness. The relatively uniform slope of the magnitude-frequency curve indicates that our HIMNT earthquake catalog is complete for events with magnitudes greater than 2.5. Event detection is not complete for events of magnitude <2.5, although many events of this size have been detected and located. Most of the earthquakes in our HIMNT catalog are not found in the global catalogs. Since the lateral variation of the velocity structure in the north-south direction is very significant in the study area, we used two different velocity models (dashed lines in Figure 4), one for the Sub-Himalaya and Lesser Himalaya (Pandey et al., 1995) and one for the southern Tibetan Plateau (Cotte et al., 1999). For earthquakes near the boundary between these two areas, the location was performed using the model corresponding to the volume through which the seismic waves predominantly propagated.

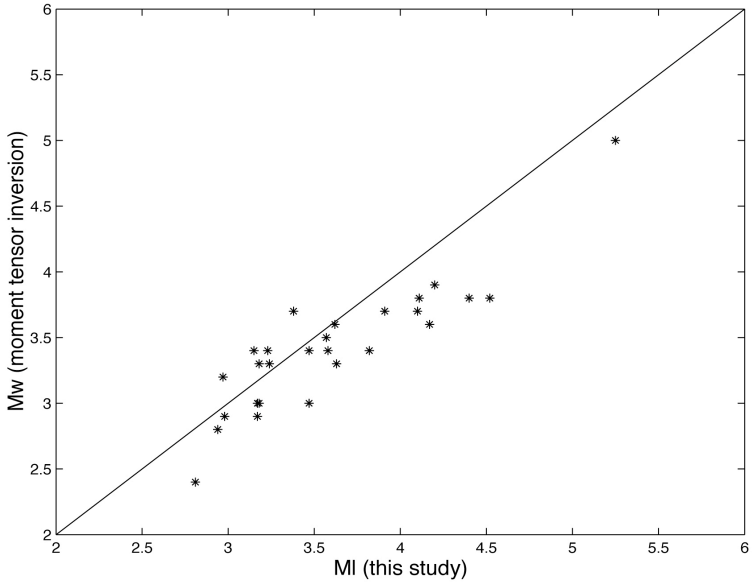


**Figure 2. Comparison between local magnitudes and moment magnitudes calculated through full waveform moment tensor inversion for a subset of earthquakes. The reference line has a slope of 1 and goes through the origin.**

## Improved velocity model and earthquake locations

The program VELEST (Kissling, 1995) was used to invert simultaneously for earthquake locations and 1D velocity structure using the arrival time data, the initial earthquake locations and a starting velocity model. After many runs with different starting models and control parameters, two velocity models, one for the Himalayas and the other for the southern Tibetan Plateau, were selected on the basis of minimum root mean square (RMS) misfit and some *a priori* information obtained from previous studies (Sapin et al., 1985; Pandey et al., 1995; Galve et al., 2002). Figure 4 shows the improved velocity models for the Himalaya of Nepal and the southern Tibetan Plateau. Using this improved velocity model, all the local earthquakes were then relocated. Figure 5 shows a map view with the earthquake relocations. Events beneath the Himalayan front show an alignment on the region of highest relief. Clusters of upper crustal earthquakes in the north part of the network are mainly related to normal faults and grabens in the southern Tibetan Plateau. A group of lower crust and upper mantle earthquakes is found beneath the Lesser Himalaya of Nepal, possibly related to the magnitude 6.5 08/20/1988 Udayapur earthquake (Pandey et al., 1999). There is also a NW-SE stripe of earthquakes in the lower crust and upper mantle beneath the Southern Tibetan Plateau and the High Himalayas. A receiver function analysis (Schulte-Pelkum et al., 2005) shows that the Moho is at most 50 km below sea level beneath the Lesser Himalaya and 75 km below sea level beneath the southern Tibetan Plateau, indicating that some of the earthquakes we located are in the upper mantle. Depths range from surface to around 65 km below sea level in the Lesser and Sub-Himalaya and from surface to around 90 km below sea level in

the High Himalaya and the southern Tibetan Plateau. No evident gaps in depth are found among the located earthquakes.

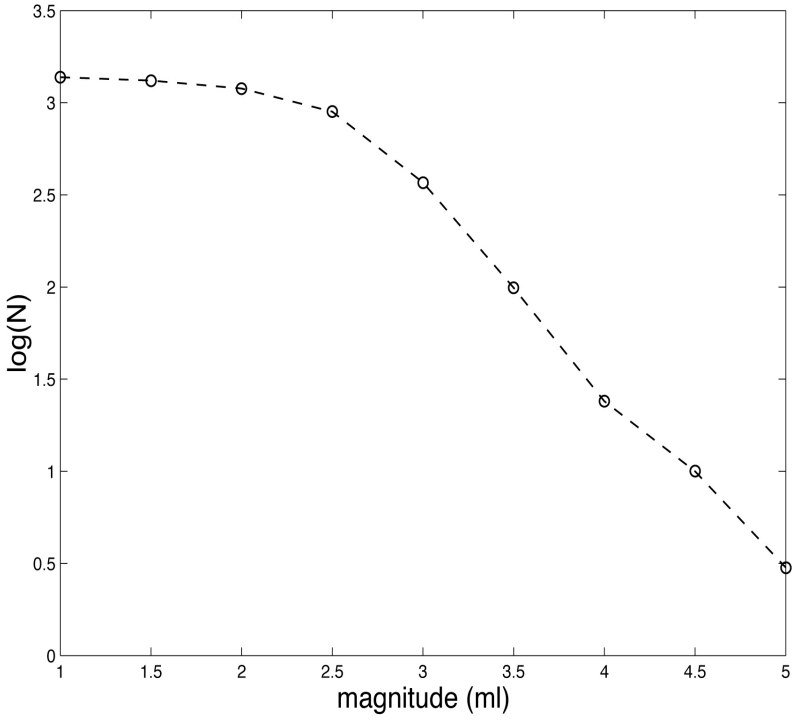


**Figure 3. Magnitude-frequency diagram for events detected and located in HIMNT network. Logarithm of the number of events greater than a certain magnitude is plotted on the vertical axis. The uniform slope for magnitudes greater than 2.5 indicates that our catalog is complete for this range of magnitudes.**

From the obtained models and the observed changes in velocity with depth, it is clear that the crust is >15 km thicker in the Tibetan Plateau than it is in the Lesser Himalaya. This greater thickness is also suggested by the receiver function analysis carried out by Schulte-Pelkum et al. (2005). These variations in crustal thickness suggest the existence of a large lateral heterogeneity in the study region, pointing out the need to invert for a 3D velocity model. A subset of 539 high-quality earthquakes was used as input to the program SIMUL2000, which relocates these earthquakes and finds a 3D velocity distribution using a damped least-squares inversion (Thurber, 1983). The study region is parameterized as a rectangular grid of nodes; SIMUL2000 iteratively inverts for P-wave velocity (Vp) at each node, P-wave velocity to S-wave velocity ratio (Vp/Vs) and earthquake location. The 1D velocity models obtained from VELEST were used as a starting model for the 3D inversion, and a succession of inversions going from coarse to finer grids was performed. The final grid has a mean node separation of about 40 km in the horizontal direction near the center of the network and 15 km in the vertical direction.

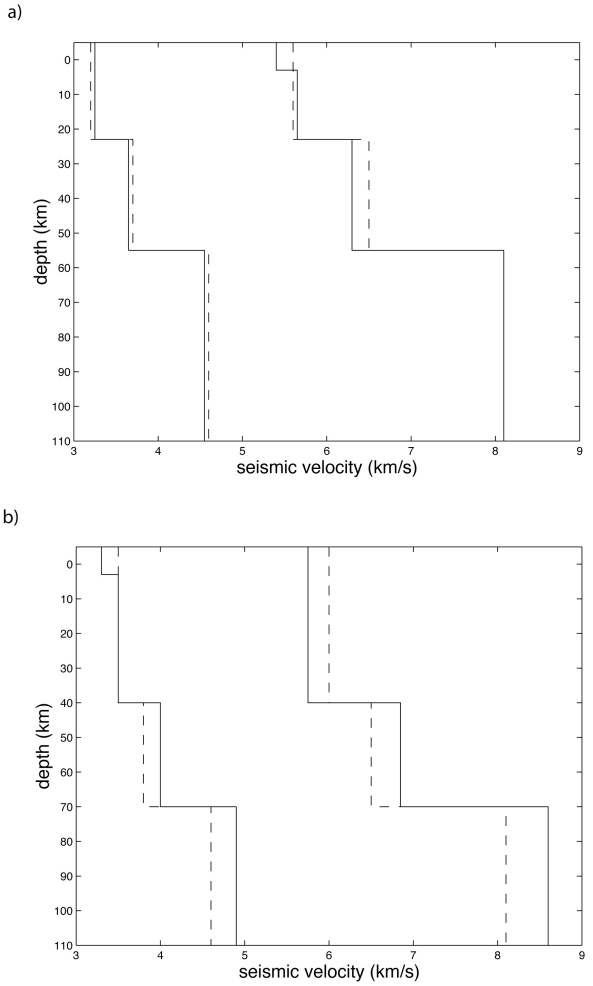


**Figure 4. The 1D velocity models used for preliminary locations (dashed lines) and the minimum-error model found with VELEST (solid lines). Layer boundaries kept fixed. (a) Results for the Lesser Himalaya (Nepal) part of the array. Initial model by Pandey et al (1995). (b) Results for the Tibetan Plateau part of the array. Initial model by Cotte et al. (1999).**

Figure 6 shows the results for Vp (6a) and Vp/Vs (6b) as horizontal slices at six different depths. Among the robust features resulting from these inversions are low values of Vp/Vs in the upper crust beneath the southern Tibetan Plateau, high P-wave velocities in the lower crust beneath the Tibetan Plateau, and high upper-mantle velocities beneath the High and Tethyan Himalayas.

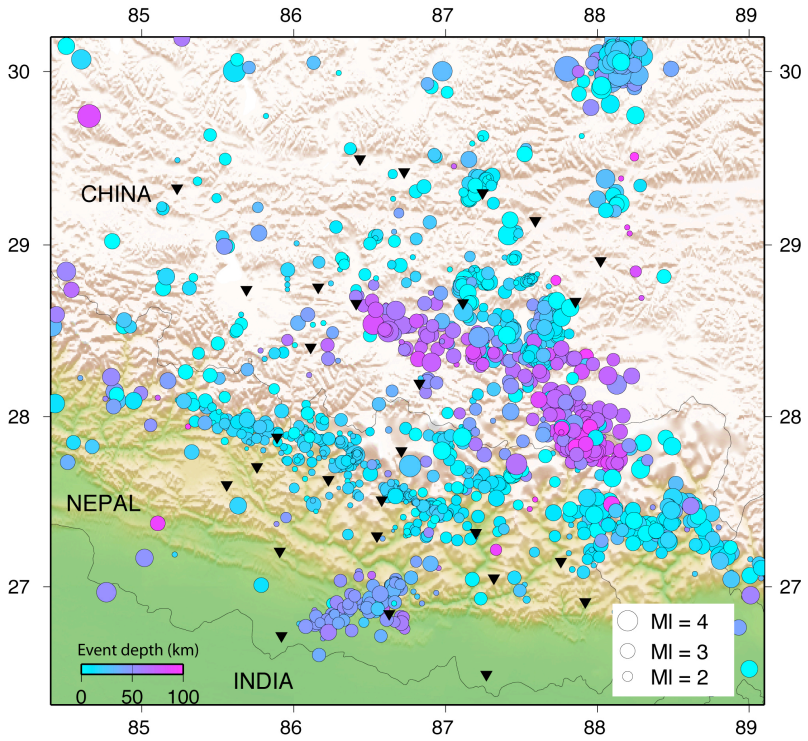


**Figure 5. Map view of earthquake locations after refining the velocity model using VELEST. The event symbol size is scaled by magnitude. Earthquakes are color scaled by depth in kilometers. Inverted triangles show HIMNT station locations. (The only stations plotted are the ones with data used here.)**

## Moment tensor and Source Parameter Analysis

We used the moment tensor inversion method of Ammon and Randall (Ammon and Randall, 1994; Randall et al., 1995; Stich et al., 2003) to calculate the deviatoric moment tensor solutions for 17 high-quality earthquakes, using data collected from the HIMNT experiment, the Bhutan PASSCAL network (Velasco, personal communication, 2004) and the Global Seismic Network (GSN, station LSA). We calculated Green's functions using two 1D velocity models, one for the Himalayas and the other for the Tibetan Plateau. The whole waveform was modeled in each inversion. We performed a grid search over depth at 5-km increments and over several overlapping bandpass ranges. The depths of minimum misfit between the data and the synthetics are in good agreement with the depths obtained by travel time inversion. Figure 7 shows observed and synthetic seismograms for a representative event, along with misfit versus depth curves calculated using several bandpasses. We also calculated first-motion focal mechanism solutions to compare to the full waveform moment tensor solutions. First motions were obtained from HIMNT data, seismograms collected from the Bhutan PASSCAL network, and the permanent short-period single-component network of the Nepal DMG.

Figures 8 and 9 illustrate the focal mechanisms in map view and cross-section respectively, along with HIMNT seismicity described in the earlier section. The moment tensor solutions for the shallow events in the southern Tibetan Plateau indicate east-west extension. Under the Himalayas, from the mid crust to the Moho, east-west extension is also present. At Moho depths and below, under the High and Tethyan Himalayas, earthquakes show normal faulting changing to strike-slip. We observed a shift in the focal mechanisms at Moho depths that indicates a change in the maximum stress through the lower crust to the upper mantle from vertical to a NW-SE/NE-SW direction.

Our GT catalog will include many of the events with moment tensor solutions. The source parameters will be provided for the GT events, and we have paid particular attention to the issue of depth control. Our waveform moment tensor solutions are improved by supplementing HIMNT data with Bhutan and GSN data, and first motion mechanism solutions use data from HIMNT, Bhutan, and the Nepal DMG network. We performed a grid search

over source depth to examine the sensitivity of the moment tensor solution to event depth and to find the best fitting source depth. Inversions were performed using a range of passbands, and sensitivity to frequency was explored. Focal mechanisms from full waveform moment tensor inversions were crosschecked with first motion solutions, and good agreement was found.

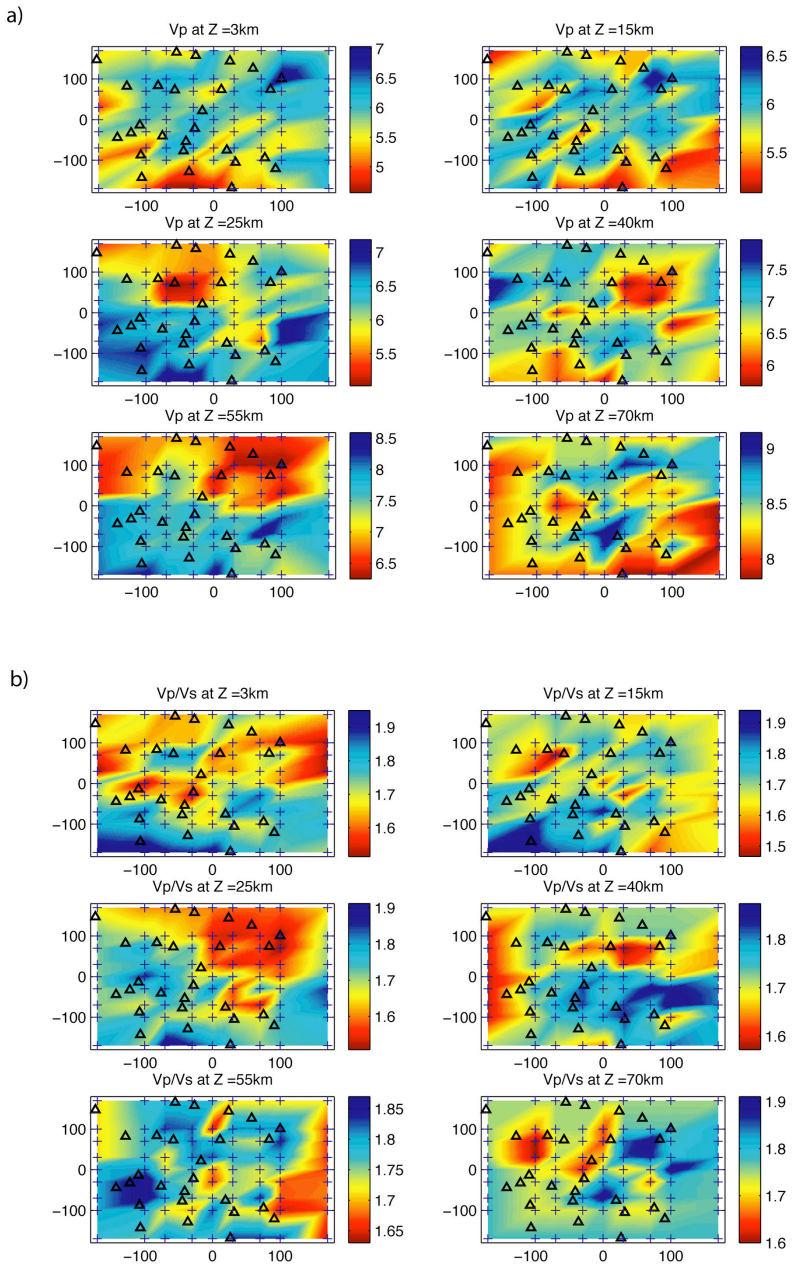


**Figure 6: Horizontal depth slices through a 3D tomography model from the application of SIMUL2000 to HIMNT P- and S-wave travel times. (a) P-wave velocity (Vp) in km/s. (b) P-wave to S-wave velocity ratio (Vp/Vs). Crosses denote inversion nodes. Black triangles represent station locations.**

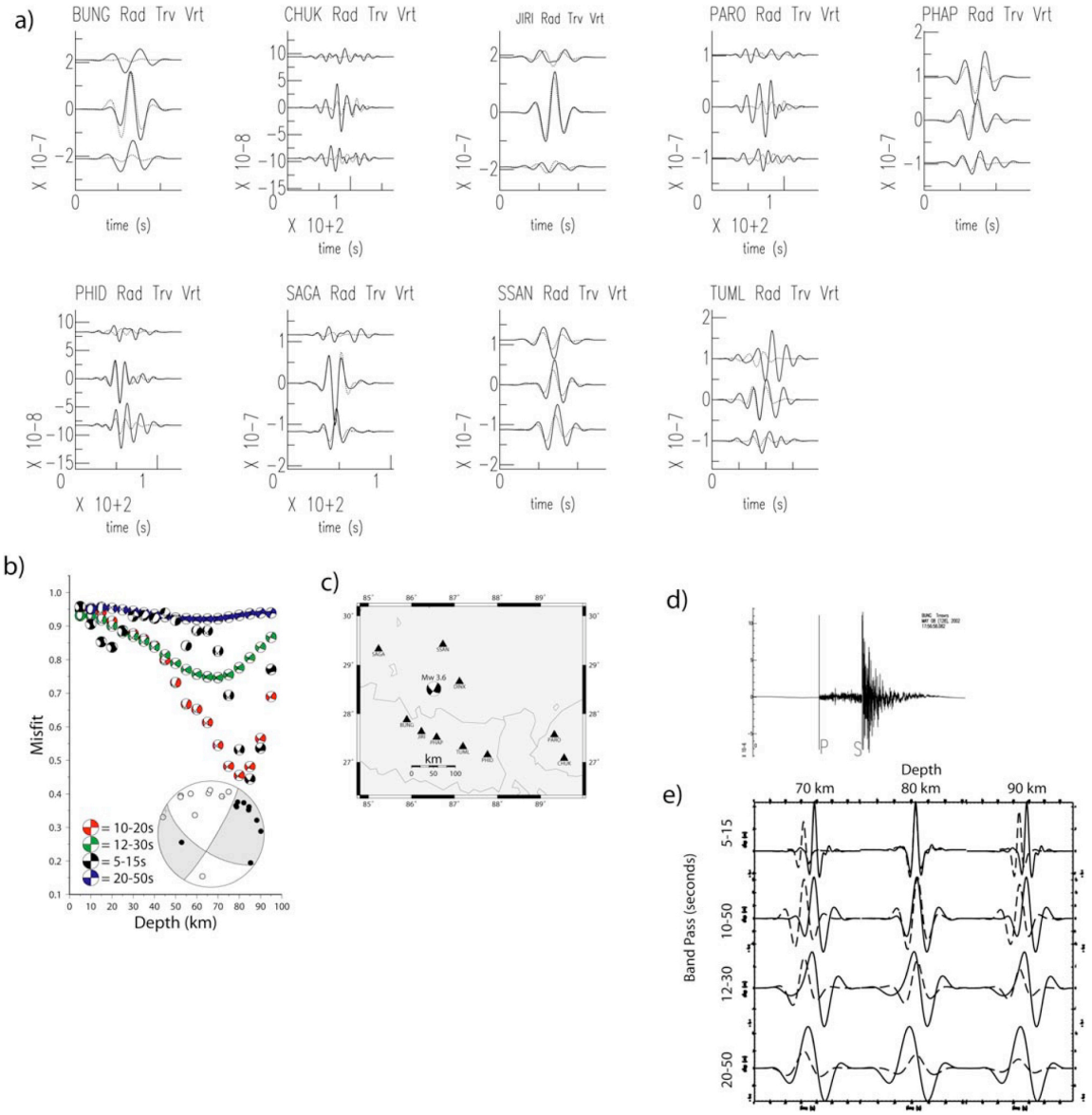


**Figure 7. Full waveform moment tensor inversion of event located at 28.5N 86.5E, depth 81 km. (a) Synthetic (dashed) and observed (solid) waveforms (10–20 s bandpass). Synthetic was calculated for the minimum misfit solution at 80 km. (b) Misfit versus depth curves for four different waveform bandpass intervals. The inset shows first-motion polarity points plotted on the best solution from moment tensor inversion. The black circles are compressions; the white circles are dilatations. The best waveform solution occurs using the 5-15 s and 10-20 s bandpass interval for an 80–85 km source depth. (c) Station locations and the best moment tensor solution plotted at event location. (d) Observed seismogram at station BUNG transverse component with P and S picks. Note the lack of surface wave energy. (e) Synthetic versus observed seismogram for synthetics calculated using source depths of 70, 80 and 90 km. Observed seismograms for bandpass intervals 5-15 s, 10-20 s, 12-30 s and 20-50 s.**

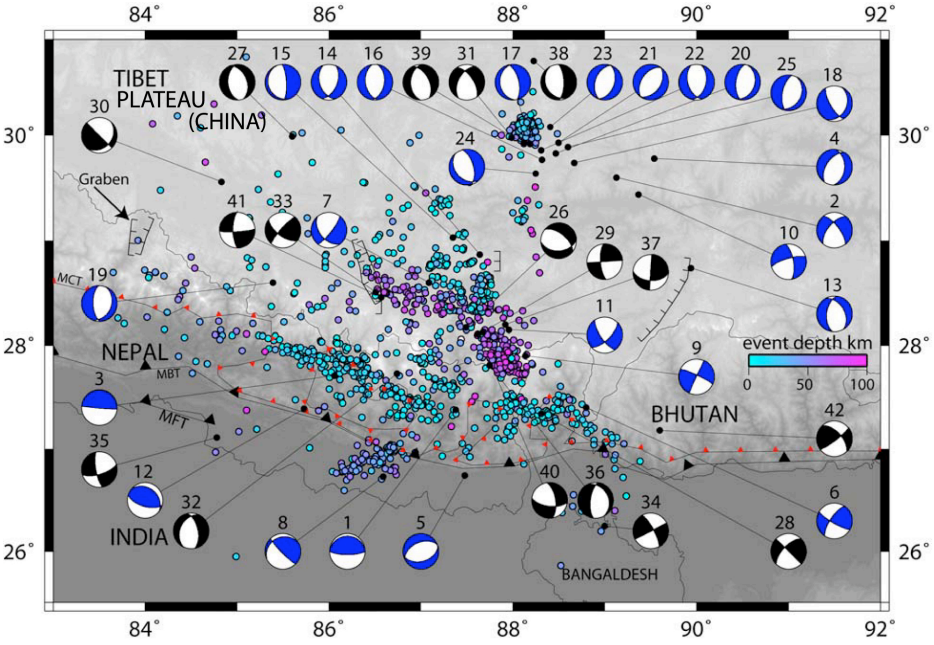


**Figure 8. Focal mechanisms from HIMNT and previous studies plotted with HIMNT seismicity from October 2001 to April 2003. Seismicity (shown as small colored circles) is color coded by depth. HIMNT focal mechanisms are shown in black. The blue focal mechanisms are from the Harvard Centroid Moment Tensor catalog and from previously published solutions (Baranowski et al., 1984; Chen et al., 1981; Chen and Yang, 2004; Molnar and Chen, 1983; Ni and Barazangi, 1984; Zhu and Helmberger, 1996). Faults shown include MCT, Main Central Thrust; MBT, Main Boundary Thrust; and MFT, Main Frontal Thrust.**

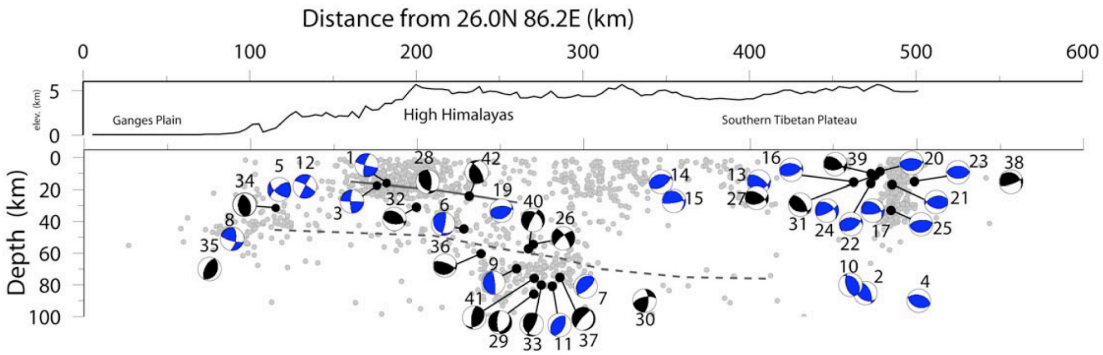


**Figure 9. Cross-section from 26.0N 86.2E azimuth 018 showing HIMNT seismicity and focal mechanisms from HIMNT and other studies. The dashed line indicates the Moho, and the solid line marks the top of the Indian Plate (Schulte-Pelkum et al., 2005). Regional topography is plotted above the seismicity. Focal mechanism colors are as in Figure 8.**

## CONCLUSION

Using in-country networks contributes to GT location determination in central Asia, which is important for validating regional velocity models and correction surfaces. Examining data from the HIMNT network indicates a wealth of high-quality events not available in global catalogs. Important steps toward the determination of precise earthquake locations, source parameters and velocity structure have been taken. Such events are of utility for GT as well as for regional velocity structure and will contribute to the National Nuclear Security Administration knowledge base.

## REFERENCES

Ammon, C. J. and G. E. Randall (1994, last updated July 2001), Moment Tensor Inversion, http://eqseis.geosc.psu.edu/~cammon/HTML/MTinvDocs/mtinv01.html (2005).

Baranowski, J., J. Armbruster, L. Seeber, and P. Molnar (1984), Focal Depths and Fault Plane Solutions of Earthquakes and Active Tectonics of the Himalaya, *J. Geophys. Res.* 89 (NB8): 6918–6928.

Chen, W. P., J. L. Nabelek, T. J. Fitch, and P. Molnar (1981), An Intermediate Depth Earthquake beneath Tibet—Source Characteristics of the Event of September 14, 1976, *J. Geophys. Res.* 86 (NB4): 2863–2876.

Chen, W. P., and Z. H. Yang (2004), Earthquakes beneath the Himalayas and Tibet: Evidence for Strong Lithospheric Mantle, *Science* 304: 1949–1952.

Cotte, N., H. Pedersen, M. Campillo, J. Mars, J. F. Ni, R. Kind, E. Sandvol, and W. Zhao (1999), Determination of the Crustal Structure in Southern Tibet by Dispersion and Amplitude Analysis of Rayleigh Waves, *Geophys. J. Int.* 138: 809–819.

Galve, A., M. Sapin, A. Hirn, J. Diaz, J. C. Lepine, M. Laigle, J. Gallart, and M. Jiang (2002), Complex Images of Moho and Variation of Vp/Vs across the Himalaya and South Tibet from a Joint Receiver-Function and Wide-Angle Reflection Approach, *Geophys. Res. Lett.* 29: 35-1–35-4.

Harvard Centroid Moment Tensor Catalog, www.seismology.harvard.edu/CMTsearch.html (2005).

Kissling, E. (1995), Program VELEST User's Guide—Short Introduction, www.sg.geophys.ethz.ch/aes/aes-html/**velest**.html .

Molnar, P., and W. P. Chen (1983), Focal Depths and Fault Plane Solutions of Earthquakes under the Tibetan Plateau, *J. Geophys. Res.* 88: 1180–1196.

Ni, J. and M. Barazangi (1984), Seismotectonics of the Himalayan Collision Zone—Geometry of the Underthrusting Indian Plate beneath the Himalaya, *J. Geophys. Res.* 89: 1147–1163.

Pandey, M. R., R. P. Tandukar, J. P. Avouac, J. Lave, and J. P. Massot (1995), Interseismic Strain Accumulation on the Himalayan Crustal Ramp (Nepal), *Geophys. Res. Lett.* 22: 751–754.

Pandey, M. R., R. P. Tandukar, J. P. Avouac, J. Vergne, and T. Heritier (1999), Seismotectonics of the Nepal Himalaya from a Local Seismic Network, *J. Asian Earth Sci.* 17: 703–712, 1999.

Randall, G. E., C. J. Ammon, and T. J. Owens (1995), Moment Tensor Estimation Using Regional Seismograms from a Tibetan Plateau Portable Network Deployment (1995), *Geophys. Res. Lett.* 22: 1665–1668.

Sapin, M., X. Wang, A. Hirn, and Z. X. Xu (1985), A Seismic Sounding in the Crust of the Lhasa Block, Tibet, *Ann. Geophys.* 3: 637–648.

Schulte-Pelkum, V., G. Monsalve, A. Sheehan, M. R. Pandey, S. Sapkota, R. Bilham, and F. Wu (2005), Imaging the Indian Subcontinent beneath the Himalaya, *Nature* 435: 1222–1225, doi:10.1038/nature03678.

Stich, D., C. J. Ammon, and J. Morales (2003), Moment Tensor Solutions for Small and Moderate Earthquakes in the Ibero-Maghreb Region, *J. Geophys. Res*. 108.

Thurber, C. H. (1983), Earthquake Locations and Three-Dimensional Crustal Structure in the Coyote Lake Area, Central California, *J. Geophys. Res.* 88: 8226–8236.

Zhu, L. P. and D. V. Helmberger (1996), Intermediate Depth Earthquakes beneath the India-Tibet Collision Zone, *Geophys. Res. Lett*. 23: 435–438.